PHYSICAL REVIEW B **88**, 155415 (2013)

Moiré minibands in graphene heterostructures with almost commensurate $\sqrt{3} \times \sqrt{3}$ hexagonal crystals

J. R. Wallbank,[1] M. Mucha-Kruczyński,[1,2] and V. I. Fal'ko[1]
[1]*Department of Physics, Lancaster University, Lancaster LA1 4YB, United Kingdom*
[2]*Department of Physics, University of Bath, Claverton Down, Bath BA2 7AY, United Kingdom*
(Received 18 June 2013; published 14 October 2013)

We present a phenomenological theory of the low-energy moiré minibands of Dirac electrons in graphene placed on an almost commensurate hexagonal underlay with a unit cell approximately three times larger than that of graphene. A slight incommensurability results in a periodically modulated intervalley scattering for electrons in graphene. In contrast to the perfectly commensurate Kekulé distortion of graphene, such superlattice perturbation leaves the zero-energy Dirac cones intact, but is able to open a band gap at the edge of the first moiré subbands, asymmetrically in the conduction and valence bands.

DOI: 10.1103/PhysRevB.88.155415 PACS number(s): 73.22.Pr, 73.21.Cd, 72.80.Vp

Two alternative methods exist to create long-period superlattices for two-dimensional (2D) electrons. One method, developed for semiconductors, is based on the lithographic patterning of the semiconductor surface.[1] The other method, highlighted by the studies of 2D atomic crystals, arises naturally from the existence of quasiperiodic moiré patterns formed by two slightly incommensurate 2D lattices with similar crystal symmetry, placed on top of each other. Graphene on hexagonal boron nitride is one example of such a heterostructure, where the effect of the moiré superlattice on 2D electrons leads to pronounced changes in the electronic properties detected by STM,[2–4] and magnetotransport experiments.[5–7]

The specific form of moiré superlattice for graphene electrons, generated by a hexagonal underlay, depends on the ratio between the periods of the two lattices and their mutual orientation. The abundance of layered hexagonal crystals and semiconductors with a hexagonal surface layer allows for a multiplicity of qualitatively different superlattice structures, with various levels of moiré supercell complexity.[8] The simplest and, by now, best studied is the highly orientated graphene-hBN heterostructure. Here we analyze the second simplest moiré pattern for Dirac electrons in graphene produced by a hexagonal underlay with an elementary unit cell approximately three times bigger than that of graphene. The effect of a perfectly commensurate $\sqrt{3} \times \sqrt{3}$ superlattice, known as the Kekulé distortion of the honeycomb lattice,[9] consists of the Bragg-type intervalley scattering of graphene electrons, which opens a gap between the conduction and valence bands. A hexagonal underlay with the lattice constant $a_S = \sqrt{3}(1+\delta)a$, $|\delta| \ll 1$, slightly different from that of the Kekulé superlattice of graphene and a small misaligned angle θ, produce a periodically oscillating intervalley coupling. Although this does not open a gap in graphene's Dirac point, it creates a specific miniband spectrum, whose generic features are studied in this paper. Below, we employ a phenomenological approach to classify the possible structure of moiré minibands of Dirac electrons in graphene[10] and, in particular, the behavior of the edge of the first minibands on the conduction- and valence-band sides.

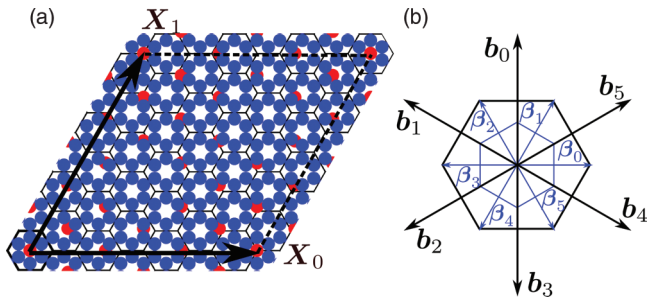

FIG. 1. (Color online) (a) The moiré pattern formed from graphene (blue) on a underlay (red) with $\theta = 0$, $\delta = \frac{1}{9}$. The black hexagons follow Kekulé lattice of graphene. (b) The two sets of reciprocal-lattice vectors, $\boldsymbol{b}_m$ and $\boldsymbol{\beta}_m$, with their associated Brillouin zones.

The image of a moiré superlattice for graphene on a substrate with a period almost commensurate with the $\sqrt{3} \times \sqrt{3}$ Kekulé lattice of graphene is shown in Fig. 1. Since graphene electrons belong to the Bloch states in their hexagonal Brillouin-zone corners and a Kekulé perturbation leads to their intervalley Bragg scattering, the symmetry of the electronic system is described by the group of wave vectors $K_\pm$, equivalent to the extended point group $C_{6v} + tC_{6v} + t^2C_{6v}$ where t is an elementary translation of the honeycomb lattice. That is why in Fig. 1(a) we show both the actual positions of carbon atoms in graphene and, using lines, the Kekulé lattice. The periodic occurrence of sites from the underlay under equivalent positions of graphene honeycomb lattice is described by a moiré pattern which is periodic under translations by X_0 and X_1. The associated reciprocal-lattice vectors belong to the set $\check{\boldsymbol{b}} = \{\boldsymbol{b}_m = \hat{R}_{2\pi m/6}\boldsymbol{b}_0\}_{m=0,\ldots,5}$ where $\hat{R}_\psi$ is the anticlockwise rotation matrix, and $\boldsymbol{b}_0 = [1-(1+\delta)^{-1}\hat{R}_\theta](0, \frac{4\pi}{\sqrt{3}a})$, so that $|\boldsymbol{b}_n| \equiv b = \frac{4\pi}{\sqrt{3}a}\sqrt{\delta^2+\theta^2}$. In contrast, the equivalent positions of substrate sites on the Kekulé lattice are characterized by the $\sqrt{3}$ times longer period of $X_0 + X_1$ and reciprocal-lattice vectors from the set $\check{\boldsymbol{\beta}} = \{\boldsymbol{\beta}_m = \frac{1}{\sqrt{3}}\hat{R}_{\frac{\pi}{2}}\boldsymbol{b}_m\}_{m=0,\ldots,5}$ with $|\boldsymbol{\beta}_n| \equiv \beta = b/\sqrt{3}$. The coexistence of these two periodicities is taken into account, on an equal footing, in the phenomenological

Hamiltonian for graphene's Dirac electrons,

$$\hat{H} = v\,\hat{\boldsymbol{p}}\cdot\boldsymbol{\sigma} + U_{E'}v\beta F(\check{\boldsymbol{\beta}})\sigma_3 + U_G v[\boldsymbol{\sigma}\times\boldsymbol{l}_z]\cdot\nabla F(\check{\boldsymbol{\beta}}) + U_{G'}v\boldsymbol{\sigma}\cdot\nabla F(\check{\boldsymbol{\beta}}) + u_0 vbf_1(\check{\boldsymbol{b}}) + u_3 vbf_2(\check{\boldsymbol{b}})\sigma_3\tau_3 + u_1 v[\boldsymbol{l}_z\times\nabla f_2(\check{\boldsymbol{b}})]\cdot\boldsymbol{\sigma}\tau_3 + u_2 v\tau_3\boldsymbol{\sigma}\cdot\nabla f_2(\check{\boldsymbol{b}}); \quad (1)$$

$$f_1(\check{\boldsymbol{v}}) = \sum_{m=0,\ldots,5} e^{i\boldsymbol{v}_m\cdot\boldsymbol{r}}, \quad f_2(\check{\boldsymbol{v}}) = i\sum_{m=0,\ldots,5}(-1)^m e^{i\boldsymbol{v}_m\cdot\boldsymbol{r}}, \quad F(\check{\boldsymbol{v}}) = f_1(\check{\boldsymbol{v}})\tau_1 + f_2(\check{\boldsymbol{v}})\tau_2.$$

This Hamiltonian is written in terms of the Pauli matrices σ_i and τ_j which act separately on the sublattice (A,B) and valley (K_+,K_-) components of the four-spinors $(\psi_{AK_+},\psi_{BK_+},\psi_{BK_-},-\psi_{AK_-})^T$ describing graphene electrons. Hence, the second line describes intravalley Bragg scattering, whereas the first line accounts for intervalley scattering. In writing $\hat{H}$, we use the earlier observation[10–15] that the potential felt by the graphene electrons is smoothed by the larger separation between graphene and the substrate than the carbon-carbon distance in graphene. For graphene on hBN, as well as twisted bilayer graphene, this resulted in the presence of only the simplest set of harmonics, $\check{\boldsymbol{b}}$, in the moiré perturbation.[10–15] For graphene on an almost commensurate $\sqrt{3}\times\sqrt{3}$ hexagonal underlay the same argument leads to the appearance of the intervalley terms. In Eq. (1), the relative strength of moiré perturbations, measured in the unit of energy $vb = \sqrt{3}v\beta$, is set by dimensionless parameters $U_{E'}$, U_G, $U_{G'}$, $u_{i=0,1,2,3}$. Here, we assume that such moiré perturbation is small, $|U_i|\ll 1, |u_j|\ll 1$, and that the underlay has an inversion-symmetric unit cell, which is a natural approximation[16] for a simple monoatomic surface layer.

To supplement a phenomenological approach to describe the moiré superlattice, Eq. (1), we also estimated parameters U_i and u_j for two limiting microscopic models: (a) the underlay is modeled as a hexagonal lattice of point charges,[10] and (b) the underlay is modeled as a lattice of atomic orbitals onto which the graphene electrons can hop (adapted from a model of twisted bilayer graphene[17]). Both models produce similar estimates for sets of phenomenological parameters U_i and u_j,

$$v\beta\{U_{E'},U_G,U_{G'}\} = \tilde{V}\left\{\frac{1}{2},\frac{-\delta}{\sqrt{\delta^2+\theta^2}},\frac{\theta}{\sqrt{\delta^2+\theta^2}}\right\},$$
$$vb\{u_0,u_1,u_2,u_3\} = \tilde{v}\left\{\frac{1}{2},\frac{-\delta}{\sqrt{\delta^2+\theta^2}},\frac{\theta}{\sqrt{\delta^2+\theta^2}},-\frac{\sqrt{3}}{2}\right\}. \quad (2)$$

However model (a) predicts $\tilde{V}\gg\tilde{v}$, whereas model (b) predicts $\tilde{V}\sim\tilde{v}$.[18]

The features of the miniband spectrum of the Dirac electrons prescribed by the intravalley terms u_j in the second line of Eq. (1) have already been explored in studies of graphene on hBN.[10–13] The characteristic feature, present in the low-energy graphene band structure for this case, consists of the formation of additional mini Dirac points[10–12] in a gapless spectrum. In contrast, intervalley perturbations U_i, are able to open gaps in the spectrum at the edges of the low-energy moiré minibands. Hence, we focus on the role of the intervalley terms, and explore the parameter space $[U_{E'},U_G,U_{G'}]$, classifying the resulting electron spectra. It is useful to notice that for the Hamiltonian in Eq. (1)

$$-\epsilon_{-U_{E'},U_G,U_{G'}}(\boldsymbol{k}) = \epsilon_{U_{E'},U_G,U_{G'}}(\boldsymbol{k}) = \epsilon_{-U_{E'},-U_G,-U_{G'}}(\boldsymbol{k}). \quad (3)$$

The first equality in Eq. (3) allows us to relate the band structure of the valence band to that of the conduction band by flipping the sign of U_E. Also, it turns out that the parameter $U_{G'}$ affects the miniband spectra of electrons only in the second order, since its first-order effect on the electron energies can be removed by the gauge transformation $\boldsymbol{\psi}\to e^{-iU_{G'}F(\check{\boldsymbol{\beta}})}\boldsymbol{\psi}'$.

The correspondence between the translational symmetries of the Hamiltonian $\hat{H}$ and the geometrical symmetry group of the moiré superlattice, $G_{SL} = \{c_6,T_{\boldsymbol{X}_0}\}$, is set by the fact that a translation, e.g., by the period $\boldsymbol{X}_0$ indicated in Fig. 1, is accompanied by a valley-dependent unitary gauge transformation, $\hat{U}_t = -\frac{1}{2} - \frac{\sqrt{3}i}{2}\tau_3$, which represents the effect of the elementary translation of the honeycomb lattice on the four-component spinors $\boldsymbol{\psi}$. This argument establishes the isomorphism of G_{SL} to the symmetry group $G_H = \{\hat{c}_6,\hat{S}_{\boldsymbol{X}_0}\}$ of the Hamiltonian $\hat{H}$, where instead of geometrical translation $T_{\boldsymbol{X}_0}$ we use $\hat{S}_{\boldsymbol{X}_0} = \hat{U}_t\hat{T}_{\boldsymbol{X}_0}$ (and $\hat{S}_{\boldsymbol{X}_1} = \hat{U}_t^\dagger\hat{T}_{\boldsymbol{X}_1}$ instead of $T_{\boldsymbol{X}_1}$). This correspondence allows one to use two equivalent descriptions of the folded mini-Brillouin zone (mBZ) of the electrons in the presence of the moiré pattern, Fig. 1(b). One, based on the longer periodicity implicit in the $e^{i\boldsymbol{\beta}_m\cdot\boldsymbol{r}}$ dependence of the intervalley part of the Hamiltonian $\hat{H}$, suggests plotting the miniband dispersion over the smaller mBZ. The other, adjusted to the periodicity of the geometrical arrangement of atoms, uses the three times larger mBZ. For the smaller mBZ, the Dirac cones from both K_+ and K_- valleys are folded onto the center of the mBZ, resulting in the valley degenerate dispersion surfaces shown in the left panel of Fig. 2(a). In contrast, the zone folding into the larger mBZ, shown in the center panel, places Dirac cones from graphene's two valleys at opposite mBZ corners. The folding of dispersion surfaces from the larger mBZ into the smaller mBZ can be used to relate the spectra shown in these alternative schemes. The unfolding of the smaller mBZ into the the larger mBZ is provided by the gauge transformation $\boldsymbol{\psi}\to U\boldsymbol{\psi}'$, $\hat{H}\to\hat{H}' = U^\dagger\hat{H}U$ where $U = e^{(i/2)(\boldsymbol{b}_0+\tau_3\boldsymbol{\beta}_0)\cdot\boldsymbol{r}}$ represents a valley dependent shift of momentum. After this gauge transformation, the new Hamiltonian $\hat{H}'$ can be written solely in terms of the $\check{\boldsymbol{b}}$ harmonics,

$$\hat{H}' = v\left(\hat{\boldsymbol{p}} + \frac{1}{6}[3\boldsymbol{b}_0 + \tau_3(\boldsymbol{b}_4+\boldsymbol{b}_5)]\right)\cdot\boldsymbol{\sigma} + U_{E'}vb(\tau_1\mathrm{Re}\,f' - \tau_2\mathrm{Im}\,f')\sigma_3 + U_G v(\tau_1\mathrm{Re}\,\boldsymbol{g}' - \tau_2\mathrm{Im}\,\boldsymbol{g}')\boldsymbol{\sigma} + U_{G'}v(\tau_1\mathrm{Re}[\hat{R}_{\pi/2}\boldsymbol{g}'] - \tau_2\mathrm{Im}[\hat{R}_{\pi/2}\boldsymbol{g}'])\boldsymbol{\sigma};$$

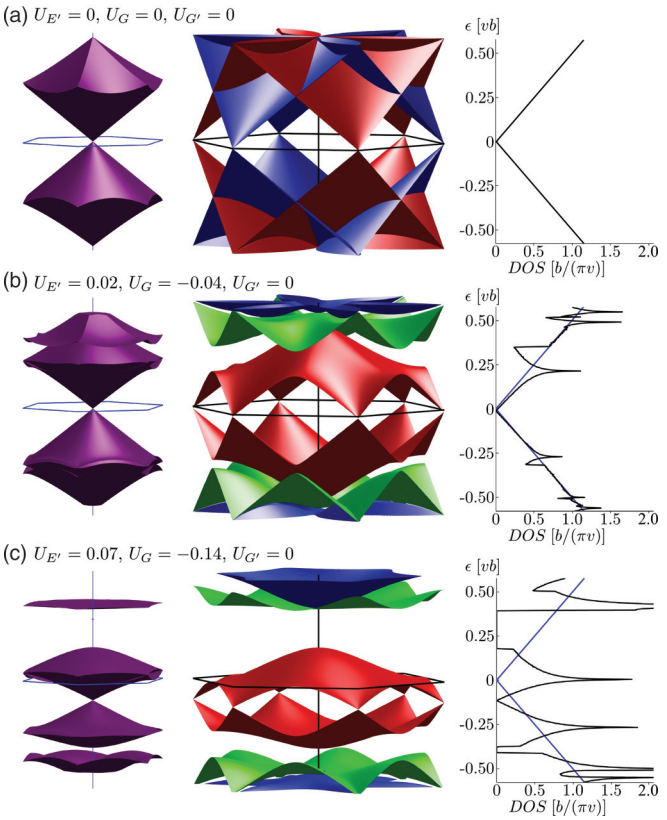

FIG. 2. (Color online) Numerically calculated moiré minibands shown in the smaller mBZ (left) and larger mBZ (center), and the corresponding density of states (right). A Van Hove singularity, originating from the first moiré miniband (in both the conduction and valence bands) is always present for the perturbed spectra.

$$f' = \frac{2}{\sqrt{3}}(1 + e^{i\boldsymbol{b}_1\cdot\boldsymbol{r}} + e^{i\boldsymbol{b}_2\cdot\boldsymbol{r}}),$$
$$\boldsymbol{g}' = \frac{2i}{\sqrt{3}}(\boldsymbol{b}_0 + \boldsymbol{b}_2 e^{i\boldsymbol{b}_1\cdot\boldsymbol{r}} + \boldsymbol{b}_4 e^{i\boldsymbol{b}_2\cdot\boldsymbol{r}}). \quad (4)$$

Characteristic miniband spectra, calculated by numerical diagonalization in the basis of zone-folded plane waves of K_+ and K_- Dirac electrons, are shown in Figs. 2(b) and 2(c). The choices of phenomenological parameters used to calculate these spectra, marked with black dots in the lower right panel of Fig. 3, correspond to the direction in the parameter space set by Eq. (2) with $\theta = 0$. Since nesting obscures some of the dispersion branches, it is useful to plot them over both the smaller mBZ (left) and the larger mBZ (middle). Also, we note that the calculated spectra will be electron-hole asymmetric, $\epsilon(\boldsymbol{k}) \neq -\epsilon(\boldsymbol{k})$, unless either $U_E = 0$ or $U_G = U_{G'} = 0$.

Generically, we find either a gapped edge of the first moiré miniband (on the conduction- and/or valence-band side of the graphene spectra) for a strong moiré perturbation, or gapless spectra with overlapping minibands for a weak moiré perturbation. In all cases, the main Dirac point is preserved with a renormalized Dirac velocity, $(1 - 12U_{E'}^2 - 24U_G^2)v$. The parameter range where the spectrum has a gap at the first miniband edge in the conduction band is shown in red in Fig. 3, whereas the parameter range with a gapless spectrum is left transparent. The magnitude of the band gap between

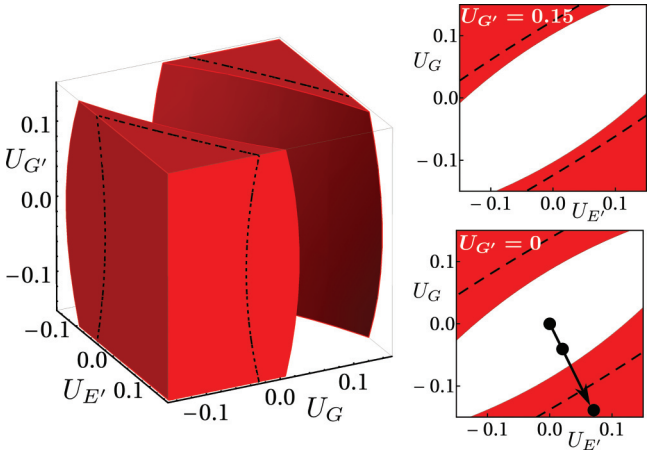

FIG. 3. (Color online) The regions of parameter space for which either an indirect band gap (within the red volume between the black dashed lines) or direct band gap (outside the black dashed lines) is present in the conduction band. The parameter space for the valence band is obtained by flipping the sign of $U_{E'}$.

the first and second minibands in either the conduction band ($s = 1$) or the valence band ($s = -1$) may be expressed in the form

$$\Delta = \frac{vb}{\sqrt{3}}\min(c,d),$$
$$c \approx \frac{-1}{2} + |4U_{E'} - 6sU_G| + \frac{4}{3}\left(U_{E'}^2 + 6sU_{E'}U_G - 2U_G^2 - 3U_{G'}^2\right),$$
$$d \approx |U_{E'} - 2sU_G| + \frac{3}{2}\left(3U_{E'}^2 - 4U_{G'}^2\right), \quad (5)$$

where $\frac{vb}{\sqrt{3}}c$ and $\frac{vb}{\sqrt{3}}d$ are the values of the indirect and direct band gaps. A negative value of Δ indicates that the bands are overlapping (no band gap, transparent volume of Fig. 3).

To summarize, Dirac electrons in graphene heterostructures, with hexagonal crystals with a unit cell approximately three times larger than that of graphene, are likely to have a band gap, Eq. (5), at the edge of the first moiré miniband, either in the conduction or valence band of graphene. This feature, and the resulting suppression of the electron density of states in graphene, take place at the energy $\epsilon_\theta \sim \pm vb/\sqrt{3}$, counted from the ungapped Dirac point. The energy scale where such a feature occurs depends on the difference between the lattice constants of the two crystals and their misalignment.

For each hexagonal crystal, the lowest possible value of ϵ_θ is shown in Table I: it corresponds to the perfect alignment of the two lattices, $\theta = 0$, and it is set by the lattice mismatch

TABLE I. Surfaces almost commensurate with the $\sqrt{3}\times\sqrt{3}$ graphene superlattice, where $\sqrt{3}a = 4.26$ Å (Ref. 27).

Surface	a_s (Å)	ϵ_0 (eV)	Band gap (eV)	Ref.
InAs(111)B	4.28	0.052	0.35	19
InP(111)B	4.15	0.290	1.34	19
$PdTe_2$	4.04	0.578	0.2	21, 20
$PtTe_2$	4.03	0.606	0.8	22, 20
InSe	4.05	0.552	≈1	23
hGaTe	4.04	0.578	2.1	24–26

δ. In this table, we list several semiconductors which can provide facets nearly commensurate with the $\sqrt{3} \times \sqrt{3}$ Kekulé superlattice in graphene. Two of them are zinc-blende-type crystals, InAs and InP, whose (111)B surfaces retain the hexagonal structure of the top layer of As or P atoms without surface reconstructions.[28–30] Of these two, InAs(111)B has a work function[31] close to that of free-standing graphene,[32] and a polar surface which causes a downward band bending, sometimes leading to an accumulation electron layer near the surface. However, it is possible to produce an accumulation-free InAs(111)B surface,[33,34] or deplete graphene-InAs using gate-controlled doping in a field-effect transistor. Due to a smaller size of the energy ϵ_0 than the InAs band gap (see Table I) it should be possible to reach the gap at the first miniband edge in graphene, before depleting states in the valence band of the InAs substrate, thus producing a graphene-based field-effect transistor with improved current on/off ratio. Since the energy of the first moiré miniband edge depends on the misalignment angle, the proposed device will work only for a limited range of (small) misalignment angles. By comparing the size of the corresponding values of ϵ_0 to the band gaps of materials in Table I, we suggest that InP(111)B, hGaTe, and InSe may also be suitable for producing a high on/off current ratio in field-effect transistors, but for $PdTe_2$ and $PtTe_2$ the band gap is too small compared to ϵ_0.

This work has been supported by EPSRC DTC NOWNANO, ERC Advanced Grant "Graphene and Beyond," Royal Society Wolfson Research Merit Award, and EPSRC Science and Innovation Award.

[1] D. K. Ferry, Prog. Quantum Electron. **16**, 251 (1992); C. Albrecht, J. H. Smet, D. Weiss, K. von Klitzing, R. Hennig, M. Langenbuch, M. Suhrke, U. Rössler, V. Umansky, and H. Schweizer, Phys. Rev. Lett. **83**, 2234 (1999); T. Schlösser, K. Ensslin, J. P. Kotthaus, and M. Holland, Europhys. Lett. **33**, 683 (1996); C. Albrecht, J. H. Smet, K. von Klitzing, D. Weiss, V. Umansky, and H. Schweizer, Phys. Rev. Lett. **86**, 147 (2001); M. C. Geisler, J. H. Smet, V. Umansky, K. von Klitzing, B. Naundorf, R. Ketzmerick, and H. Schweizer, *ibid*. **92**, 256801 (2004).

[2] S. Marchini, S. Günther, and J. Wintterlin, Phys. Rev. B **76**, 075429 (2007).

[3] A. T. N'Diaye, J. Coraux, T. N. Plasa, C. Busse, and T. Michely, New J. Phys. **10**, 043033 (2008).

[4] R. Decker, Y. Wang, V. W. Brar, W. Regan, H. Tsai, Q. Wu, W. Gannett, A. Zettl, and M. F. Crommie, Nano Lett. **11**, 2291 (2011).

[5] L. A. Ponomarenko, R. V. Gorbachev, G. L. Yu, D. C. Elias, R. Jalil, A. A. Patel, A. Mishchenko, A. S. Mayorov, C. R. Woods, J. R. Wallbank, M. Mucha-Kruczynski, B. A. Piot, M. Potemski, I. V. Grigorieva, K. S. Novoselov, F. Guinea, V. Falko, and A. K. Geim, Nature (London) **497**, 594 (2013).

[6] C. R. Dean, L. Wang, P. Maher, C. Forsythe, F. Ghahari, Y. Gao, J. Katoch, M. Ishigami, P. Moon, M. Koshino, T. Taniguchi, K. Watanabe, K. L. Shepard, J. Hone, and P. Kim, Nature (London) **497**, 598 (2013).

[7] B. Hunt, J. D. Sanchez-Yamagishi, A. F. Young, M. Yankowitz, B. J. LeRoy, K. Watanabe, T. Taniguchi, P. Moon, M. Koshino, P. Jarillo-Herrero, and R. C. Ashoori, Science **340**, 1427 (2013).

[8] The generalization of this study to substrates with other near commensurate periods (na or $n\sqrt{3}a$) will be considered elsewhere.

[9] V. V. Cheianov, V. Falko, O. Syljuåsen, and B. L. Altshuler, Solid State Commun. **149**, 1499 (2009).

[10] J. R. Wallbank, A. A. Patel, M. Mucha-Kruczynski, A. K. Geim, and V. I. Fal'ko, Phys. Rev. B **87**, 245408 (2013).

[11] M. Yankowitz, J. Xue, D. Cormode, J. D. Sanchez-Yamagishi, K. Watanabe, T. Taniguchi, P. Jarillo-Herrero, P. Jacquod, and B. J. LeRoy, Nat. Phys. **8**, 382 (2012).

[12] C. Ortix, L. Yang, and J. van den Brink, Phys. Rev. B **86**, 081405 (2012).

[13] M. Kindermann, B. Uchoa, and D. L. Miller, Phys. Rev. B **86**, 115415 (2012).

[14] J. M. B. Lopes dos Santos, N. M. R. Peres, and A. H. Castro Neto, Phys. Rev. Lett. **99**, 256802 (2007); Phys. Rev. B **86**, 155449 (2012).

[15] R. Bistritzer and A. H. MacDonald, Phys. Rev. B **81**, 245412 (2010); **84**, 035440 (2011).

[16] Inversion asymmetric terms may be included in Eq. (1) by adding terms with $f_1(\check{\boldsymbol{v}}) \to f_2(-\check{\boldsymbol{v}})$ and $f_2(\check{\boldsymbol{v}}) \to f_1(-\check{\boldsymbol{v}})$.

[17] M. Kindermann and P. N. First, Phys. Rev. B **83**, 045425 (2011).

[18] For the point-charge model (Ref. 10), $\tilde{V} = I[4\pi/(3a)]$, $\tilde{v} = I[4\pi/(\sqrt{3}a)]$, $I(g) \approx \frac{8\pi|e|Q}{9a^4\epsilon} \int dq_z dq_z' \frac{\psi^*(\boldsymbol{K},q_z)e^{i(q_z-q_z')\cdot d}\psi(\boldsymbol{K},q_z')}{g^2+(q_z-q_z')^2}$. Here Q is the charge per substrate lattice site, D is the graphene-substrate distance, ϵ is the electric permittivity, and $\psi(\boldsymbol{Q},q_z)$ is the Fourier transform of the graphene P^z orbitals. For the hopping model $\tilde{V} = \tilde{v} = \frac{-\gamma^2}{9\epsilon_s}$ with γ the hopping integral to the substrate and ϵ_s the energy of the substrate state.

[19] *Semiconductors: Group IV Elements and III-V Compounds*, Data in Science and Technology series, edited by O. Madelung (Springer-Verlag, Berlin, 1991), Secs. 2.13–2.14.

[20] S. Lebegue, T. Bjorkman, M. Klintenberg, R. M. Nieminen, and O. Eriksson, Phys. Rev. X **3**, 031002 (2013).

[21] J. A. Wilson and A. D. Yoffe, Adv. Phys. **18**, 193 (1969).

[22] S. Furuseth, K. Selte, and A. Kjeksiius, Acta Chem. Scand. **19**, 257 (1965).

[23] J. V. McCanny and R. B. Murray, J. Phys. C: Solid State Phys. **10**, 1211 (1977).

[24] V. Zólyomi, N. D. Drummond, and V. I. Fal'ko, Phys. Rev. B **87**, 195403 (2013).

[25] S. A. Semiletov and V. A. Vlasov, Sov. Phys. Crystallogr. **8**, 704 (1964).

[26] E. G. Gillan and A. R. Barron, Chem. Mater. **9**, 3037 (1997).

[27] A. H. Castro Neto, F. Guinea, N. M. R. Peres, K. S. Novoselov, and A. K. Geim, Rev. Mod. Phys. **81**, 109 (2009).

[28] C. B. M. Andersson, U. O. Karlsson, M. C. Hakansson, L. O. Olsson, L. Ilver, J. Kanski, P.-O. Nilsson, and P. E. S. Persson, Surf. Sci. **307–309**, 885 (1994).

[29]X.-Y. Hou, G.-S. Dong, X.-M. Ding, and X. Wang, Surf. Sci. **183**, 123 (1987).
[30]S. Mankefors, P. O. Nilsson, and J. Kanski, Surf. Sci. **443**, L1049 (1999).
[31]K. Szamota-Leandersson, M. Gothelid, J. Kanski, L. Ilver, G. Le Lay, and U. O. Karlsson, Phys. Rev. B **74**, 205406 (2006).
[32]Y.-J. Yu, Y. Zhao, S. Ryu, L. E. Brus, K. S. Kim, and P. Kim, Nano Lett. **9**, 3430 (2009).
[33]Y. Fukuda, S. Ichikawa, M. Shimomura, N. Sanada, and Y. Suzuki, Vacuum **67**, 37 (2002).
[34]M. J. Lowe, T. D. Veal, A. P. Mowbray, and C. F. McConville, Surf. Sci. **544**, 320 (2003).